Signal Processing 158 (2019) 26–35

Contents lists available at ScienceDirect

Signal Processing

journal homepage: www.elsevier.com/locate/sigpro

Performance analysis of the reference signal reconstruction for DVB-T passive radars

Osama Mahfoudia [a,b,*], François Horlin [b], Xavier Neyt [a]

[a] Royal Military Academy, Rue Hobbema 8, Brussels 1000, Belgium
[b] Université libre de Bruxelles, Avenue Franklin Roosevelt 50, Brussels 1050, Belgium

ARTICLE INFO

Article history:
Received 17 April 2018
Revised 19 December 2018
Accepted 21 December 2018
Available online 25 December 2018

Keywords:
Passive radars
DVB-T
Signal reconstruction

ABSTRACT

The present work investigates the reference signal reconstruction method for passive coherent location (PCL) radars exploiting Digital Video Broadcasting-Terrestrial (DVB-T) signals. The reference signal reconstruction improves the signal-to-noise ratio (SNR) of the reference signal, which enhances the detection probability for DVB-T based PCL systems. The existing approach for the reference signal reconstruction is performed by demodulating the received reference signal to retrieve the transmitted quadrature amplitude modulation (QAM) symbols and modulate them to obtain the reconstructed signal. For low SNR values, the QAM symbol detection is accompanied with a significant error, which leads to a mismatch between the reconstrued signal and the exact one. Consequently, the expected improvement due to the signal reconstruction is limited. In this work, we propose an optimum reconstruction method which filters the detected QAM symbol prior to the remodulation step. To validate the proposed method, we retrieved analytic expressions for the detection and false-alarm probabilities and verified them through Monte-Carlo simulations. In addition, real-data sets were used to evaluate the proposed method performances. The results show that the proposed method outperforms the conventional one by extending the feasibility of the reference signal reconstruction for low SNR values.

1. Introduction

Passive coherent location (PCL) radars exploit non-cooperative signal sources as illuminators of opportunity to detect targets [1]. This silent operating mode circumvent the need of a dedicated transmitter part. Consequently, a significant reduction of the operating cost is expected compared to active radars. Another major advantage of the PCL radars is their immunity against interception and hostile enemy actions [2,3].

The exploited illuminators of opportunity in PCL radars can be another radar or a commercial transmitter. A special interest has been accorded to telecommunication and broadcasting signals as illuminators of opportunity, such as frequency modulation (FM) radio [4–6], global system for mobile communications (GSM) [7,8], digital audio broadcasting (DAB) [9,10], and digital video broadcasting-terrestrial (DVB-T) [11,12]. The suitability of these illumination sources for PCL radars can be evaluated by analyzing the transmitted waveforms (bandwidth and ambiguity function) and the transmitted power which is key factor for the definition of the detection range.

Bistatic PCL systems employ two receiving channels: a reference channel and a surveillance channel. The reference channel acquires the direct-path signal from the illuminator of opportunity, and the surveillance channel collects the target echoes [12]. The most popular detection method for PCL radars is the cross-correlation (CC). The CC detector is an imitation of the matched-filter (MF) approach with the exception that the MF employs the exact waveform and the CC uses the received reference signal. The detection is performed by cross-correlating the surveillance signal with a time-delayed and frequency-shifted copy of the reference signal for all the considered range-velocity values, which results a range-Doppler diagram [12].

The distance separating the receiver and the illuminator of opportunity can be considerable, which degrades the signal-to-noise ratio (SNR) of the reference signal. Similarly, multipath and interferences may degrade the reference signal quality. Therefore, a performance degradation of the CC detector compared to the MF is expected. The impact of the reference signal noise on the detection performance has been addressed in many studies [13–17]. It increases the detection noise floor, which buries low-power target echoes and degrades the detection probability.

* Corresponding author at: Royal Military Academy, Rue Hobbema 8, Brussels 1000, Belgium.
E-mail address: osama.mahfoudia@gmail.com (O. Mahfoudia).

https://doi.org/10.1016/j.sigpro.2018.12.016
0165-1684/

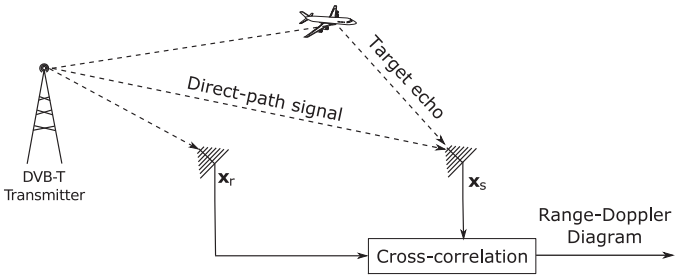

Fig. 1. Bistatic PCL configuration.

DVB-T signals are widely used as illuminators of opportunity for PCL radars. They are characterized by a bandwidth of 7.61 MHz which allows a range resolution of about 40 m, and a relatively high radiated power (about 10 kW) which permits medium-range surveillance applications [2]. In addition, the well-known structure of the DVB-T signal allows the reconstruction of the reference signal to enhance its SNR [9,11,12,18–20]. In the reference signal reconstruction process, the received signal is decoded to retrieve the transmitted quadrature amplitude modulation (QAM) symbols which are used to form a noise-free reference signal.

An accurate decoding of the DVB-T signal requires a relatively high SNR value [21]. Otherwise, the QAM detection error will be considerable, which results a mismatch between the reconstructed signal and the exact one. This signal mismatch reduces the coherent processing gain and thus degrades the detection probability. Therefore, the performance of the reference signal reconstruction strategy is limited for insufficient SNR values.

In this work, we carry out an analytic modeling of the reference signal reconstruction for DVB-T based PCL systems, which yields closed-form expressions for detection and false-alarm probabilities. These expressions permit an accurate assessment of the signal reconstruction performances and its limitations in terms of detection probability improvement. In addition, we propose an optimum signal reconstruction method [22] which considers the QAM symbol detection error and optimally filters the detected QAM symbols to reduce the reconstruction mismatch. To validate the analytic expressions, we perform Monte-Carlo simulations and we show real-data results.

The paper is organized as follows. Section 2 describes the signal model for received and DVB-T signals. In Section 3, we present the conventional signal reconstruction method, and we introduce the optimum reconstruction approach. Section 4 describes the statistical analysis which yields to closed-form expressions for the signal reconstruction performances. The results and discussion are presented in Section 5. Finally, Section 6 concludes the paper.

2. Signal model

In this section, we first define the model of the received signals (reference and surveillance signals). Then, we present the DVB-T signal structure and its statistical model.

2.1. Received signals

In this work, we consider a bistatic PCL system based on the DVB-T illumination as presented in Fig. 1, and we adopt the simplified signal model employed in [13,16] to express the reference and surveillance signals.

The reference channel antenna is steered towards the illuminator of opportunity to capture the direct-path signal. If we neglect the contribution of interferences and multipath components, the reference signal can be expressed as

$$x_r(n) = \beta s(n) + v(n), \tag{1}$$

where $s(n)$ is the signal transmitted by the illumination source with a variance of σ_s^2, β is a complex parameter which represents the propagation losses and the antenna gain, and $v(n)$ is a thermal noise following a complex Gaussian distribution of zero mean and variance σ_v^2, i.e., $v(n) \sim \mathcal{CN}(0, \sigma_v^2)$. Thus, the signal-to-noise ratio of the received reference signal can be expressed as follows

$$\mathrm{SNR_r} = |\beta|^2 \sigma_s^2 / \sigma_v^2. \tag{2}$$

For real scenarios, the reference signal may include interferences, multipath, or signals from transmitters operating in a single frequency mode (SFN). To cope with these disturbance sources, an efficient directive antenna or beamforming architectures can be employed. The considered model for the current paper exclusively emphasizes the noise contribution since our principal subject is the noise impact assessment.

The surveillance channel antenna is directed towards the surveillance area. In addition to the target echoes, the surveillance channel captures direct-path and multipath signals. The received surveillance signal $x_s^i(n)$ can be expressed as a binary hypothesis model [12,23]

$$\begin{cases} \mathrm{H}_0 : x_s^i(n) = \sum_{l=0}^{L-1} h_l s(n-l) + w_0(n), \\ \mathrm{H}_1 : x_s^i(n) = \sum_{l=0}^{L-1} h_l s(n-l) + \alpha s(n-\tau) e^{j2\pi f_d n} + w_0(n). \end{cases} \tag{3}$$

For the null hypothesis (H_0), the surveillance signal includes a direct-path components ($h_0 s(n)$), $L-1$ multipath components and a thermal noise $w_0(n)$. Each multipath component is characterized by a time delay l and a propagation gain h_l, this undesirable contribution (together with the direct-path signal) is known as the static clutter. In addition to the static clutter and the thermal noise, the surveillance signal under the alternative hypothesis (H_1) includes a target echo which is modeled as an attenuated, time-delayed, and frequency-shifted copy of the transmitted signal. The time-delay τ reflects the target bistatic range, and the frequency-shift f_d results from the target bistatic velocity. The complex attenuation α, which we consider constant during the coherent processing interval, stands for the antenna gain, the propagation losses and the target reflectivity.

The static-clutter contribution can be mitigated by directing the antenna nulls towards the transmitter of opportunity and the major static scatterers, or by employing a static clutter suppression method [24–26]. The resulting surveillance signal $x_s(n)$, after static clutter suppression, can be expressed as a binary hypothesis model

$$\begin{cases} \mathrm{H}_0 : x_s(n) = w(n), \\ \mathrm{H}_1 : x_s(n) = \alpha s(n-\tau) e^{j2\pi f_d n} + w(n), \end{cases} \tag{4}$$

with the term $w(n)$ involves the thermal noise ($w_0(n)$) and the residual direct-path and multipath signals. We assume that $w(n)$ follows a complex Gaussian distribution with zero mean and variance σ_w^2, i.e., $w(n) \sim \mathcal{CN}(0, \sigma_w^2)$. The signal-to-noise ratio in the surveillance signal can be expressed as

$$\mathrm{SNR_s} = |\alpha|^2 \sigma_s^2 / \sigma_w^2. \tag{5}$$

2.2. DVB-T signal

The DVB-T standard adopts a multicarrier modulation scheme called orthogonal frequency division multiplexing (OFDM). The DVB-T signal is organized into symbols, each symbol is formed by a large number of orthogonal and closely spaced subcarriers [27]. The time-domain signal model for one DVB-T symbol employing K subcarriers is obtained as follows

$$s(n) = \sum_{k=0}^{K-1} c_k e^{j2\pi f_k n}, \tag{6}$$

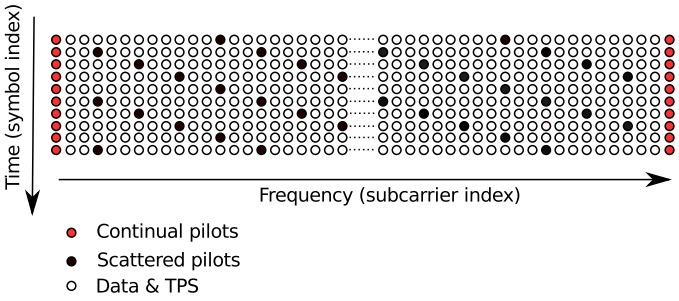

Fig. 2. DVB-T frame structure showing the pilot subcarrier distribution.

Table 1
Main parameters of the DVB-T signal.

Parameter	2 K mode	8 K mode
Number of subcarriers K	1705	6817
Number of data subcarriers K_d	1512	6048
Number of pilot subcarriers K_p	176	701
Number of TPS subcarriers K_{TPS}	17	68
Useful symbol duration T_U	224 μs	896 μs
Subcarrier spacing Δf	4464 Hz	1116 Hz
Signal bandwidth B	7.61 MHz	7.61 MHz

where f_k is the frequency of the kth subcarrier and c_k is the kth QAM symbol. Equivalently, we can express the DVB-T signal for one symbol duration as

$$\mathbf{s} = \mathbf{F}^{-1}\mathbf{c}, \tag{7}$$

where $\mathbf{F}$ is the discrete Fourier transform (DFT) matrix ($K \times K$), and $\mathbf{c}$ is the QAM symbol array ($K \times 1$) defined as follows

$$\mathbf{c} = [c_0, c_1, c_2, \ldots, c_{K-1}]^T. \tag{8}$$

The DVB-T signal is obtained through an inverse DFT of independent coded symbols c_k. Knowing that the IDFT of statistically independent inputs produces statistically independent outputs [28], and since the sum of a large number of independent and identically distributed (i.i.d) variables approaches a Gaussian distribution (invoking the central limit theorem CLT), we can consider that the transmitted DVB-T signal $s(n)$ is following a complex Gaussian distribution with zero mean and variance σ_s^2, i.e., $s(n) \sim \mathcal{CN}(0, \sigma_s^2)$ [28–30].

Fig. 2 presents the frame structure for DVB-T signals, it shows the different subcarrier categories. Three categories are emphasized: data subcarriers, transmission parameter signaling (TPS) subcarriers, and pilot subcarriers. Data subcarriers convey video coded data, and TPS subcarriers transport transmission parameters. Pilot subcarriers are used for signal synchronization and propagation channel estimation; they are transmitted at known frequencies and with known amplitudes.

Table 1 presents the main parameters of the DVB-T standard for both transmission modes 2 K and 8 K such as the number of the involved subcarriers, the number of data, pilot and TPS subcarriers. We note that the positions of data, pilot and TPS subcarriers are known and can be determined for each DVB-T symbol [27]. Hence, we note Ω_{d} ($K_d \times 1$) and Ω_{p} ($K_p \times 1$) the arrays involving the data and pilot subcarrier indices, respectively. It follows that if we neglect the TPS subcarriers and consider the manimupalting matrix $\mathbf{A}$, the QAM vector presented in (8) can be expressed as

$$\mathbf{c_m} = \begin{pmatrix} \mathbf{c}_{\text{d}} \\ \mathbf{c}_{\text{p}} \end{pmatrix}, \tag{9}$$

where $\mathbf{c}_{\text{d}}$ ($K_d \times 1$) is the data symbol array and $\mathbf{c}_{\text{p}}$ ($K_p \times 1$) is the pilot symbol array. This result is obtained by considering the following transformation

$$\mathbf{c_m} = \mathbf{A}\,\mathbf{c}, \tag{10}$$

where the matrix $\mathbf{A}$ is expressed as

$$\mathbf{A} = \begin{pmatrix} \mathbf{A_d} \\ \mathbf{A_p} \end{pmatrix}, \tag{11}$$

with the elements of $\mathbf{A_d}$ ($K_d \times 1$) and $\mathbf{A_p}$ ($K_p \times 1$) are calculated as

$$\mathbf{A_d}(l, m) = \begin{cases} 1 & \text{if } \Omega_{\text{d}}(l) = m, \\ 0 & \text{otherwise}, \end{cases} \tag{12}$$

and

$$\mathbf{A_p}(l, m) = \begin{cases} 1 & \text{if } \Omega_{\text{p}}(l) = m, \\ 0 & \text{otherwise}. \end{cases} \tag{13}$$

Pilot subcarriers form approximately 10% of the employed subcarriers: 176/1705 for 2 K mode and 701/6817 for 8 K mode. They are modulated by a pseudo-random binary sequence (PRBS) generator, which yields binary phase shift keying (BPSK) symbols ($\pm 4/3$). Let us call $p(n)$ the pilot signal which results from the sum of the pilot subcarrier time-domain signals. In [31,32], it has been shown that for a large number of subcarriers ($K > 100$), the central limit theorem (CLT) can be invoked over the IDFT result. Hence, we can assume that $p(n)$ follows a complex Gaussian distribution with zero mean and variance σ_p^2, i.e., $p(n) \sim \mathcal{CN}(0, \sigma_p^2)$. Likewise, we call $d(n)$ the sum of time-domain data subcarrier signals. The data subcarriers are loaded by QAM symbols which are mapped from randomized binary data. Consequently, the resulting QAM symbols are independent and identically distributed. Therefore, we can consider (by invoking the CLT) that the data signal $d(n)$ follows a complex Gaussian distribution with zero mean and variance σ_d^2, i.e., $d(n) \sim \mathcal{CN}(0, \sigma_d^2)$. Thus, we can write the DVB-T signal as the sum of two components

$$s(n) = d(n) + p(n), \tag{14}$$

and since the data signal $d(n)$ and the pilot signal $p(n)$ are statistically independent, we can write

$$\sigma_s^2 = \sigma_d^2 + \sigma_p^2. \tag{15}$$

We define the ratio between the data signal and the pilot signal powers as follows

$$\rho = \sigma_d^2 / \sigma_p^2, \tag{16}$$

the parameters σ_d^2, σ_p^2, and ρ are known for a given DVB-T transmission mode (2K and 8K).

The pilot signal can be employed to estimate the signal-to-noise ratio in the reference signal (SNR_{r}) [33] as follows

$$\hat{\text{SNR}}_{\text{r}} = \frac{|\hat{\beta}|^2(1+\rho)\sigma_p^2}{r_x - |\hat{\beta}|^2(1+\rho)\sigma_p^2}, \tag{17}$$

where r_x is the received signal power calculated by

$$r_x = \text{E}[x_r(n)x_r^*(n)], \tag{18}$$

and $\hat{\beta}$ is the estimate of the parameter β in Eq. (1), calculated as follows

$$\hat{\beta} = r_{xp}/\sigma_p^2, \tag{19}$$

with

$$r_{xp} = \text{E}[x_r(n)p^*(n)]. \tag{20}$$

3. Signal reconstruction

As mentioned in the introduction, the DVB-T signal structure permits the reconstruction of the reference signal to enhance its quality by rejecting the accompanying noise. The DVB-T signal reconstruction includes a demodulation followed by a modulation

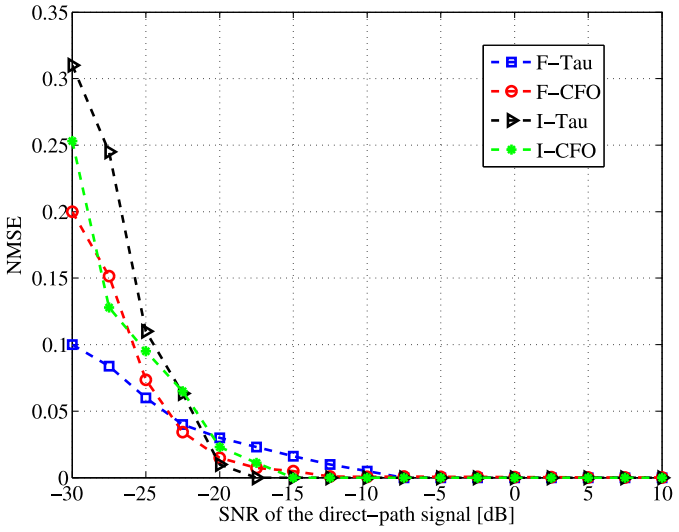

Fig. 3. Normalized mean square error of the DVB-T signal synchronization stages as a function of the signal SNR with F-Tau is the fractional time offset, F-CFO is the fractional CFO, I-Tau is the integer time offset and I-CFO integer CFO.

operations. The demodulation of the DVB-T signal is structure-based which requires an accurate time and frequency synchronization of the received signal. In this section, we first discuss the DVB-T signal synchronization stages and the impact of the signal quality on their efficiency. Then, we present the conventional and optimum approaches for the reference signal reconstruction in the DVB-T based PCL radars.

3.1. Signal synchronization

As was stated earlier, the DVB-T signal demodulation is preceded by the imperative synchronization stages. Due to its importance, the synchronization of OFDM signals (such as DVB-T signals) have been considered as the subject of many studies [34–39]. The DVB-T signal synchronization deals with four uncertainties which are the unknown begging of each DVB-T symbol (fractional time offset), the pattern of the pilot subcarrier pilots (integer time offset) and the carrier frequency offset (CFO) with its fractional and integer parts [34].

In this work, we consider the signal synchronization algorithms presented in [34] and we evaluate their efficiency for low SNR values. In Fig. 3, we present the normalized mean square error (NMSE) related to the four synchronization stages, where a signal of length $N = 10^6$ is considered. The results show that for SNR > -20 dB, an NMSE level lower than 0.02 can be achieved which is an accepted rate. In addition, the synchronization performance can be improved by considering a larger signal length since the synchronization stages are correlation based. Therefore, we consider that the synchronization quality enables an accurate demodulation of the DVB-T signal for low SNR scenarios.

3.2. Conventional reconstruction

As was stated in the introduction, the process of the reference signal reconstruction involves a decoding step which provides an estimation of the transmitted QAM symbols. Prior to the signal decoding, time and frequency synchronization of the received signal are required as shown earlier [27]. Time synchronization retrieves the beginning of the DVB-T symbols; it employs the guard interval correlation. For the frequency synchronization, the pilot subcarriers are employed to compensate the carrier frequency offset. Note that if the reference channel involves multipath signals, the propagation channel estimation is needed to equalize the received QAM symbols [37].

The synchronized signal is divided into DVB-T symbols and the guard interval (GI) is removed from each symbol. To retrieve the frequency-domain components, the DFT is applied as follows

$$\mathbf{c}_\mathrm{r} = \mathbf{F}\mathbf{x}_\mathrm{r}, \tag{21}$$

where $\mathbf{F}$ is the DFT matrix and $\mathbf{x}_\mathrm{r}$ is the synchronized reference signal after GI removal.

For a flat propagation channel, the symbol detection of $\mathbf{c}_\mathrm{r}$ provides an estimate of the transmitted symbols for data and pilot subcarriers, which we note $\hat{\mathbf{c}}$. Since data subcarriers convey QAM symbols, their detection accuracy depends on the SNR_r level. In contrast, the amplitudes of pilot subcarriers (BPSK) are known at the receiver and thus can be perfectly reconstructed independently of the SNR_r level. Therefore, the detected symbols $\hat{\mathbf{c}}$ are expressed as follows

$$\hat{\mathbf{c}}_\mathbf{m} = \begin{pmatrix} \hat{\mathbf{c}}_\mathrm{d} \\ \mathbf{c}_\mathrm{p} \end{pmatrix}, \tag{22}$$

where $\hat{\mathbf{c}}_\mathrm{d}$ expresses the detected data symbols (QAM). The reference signal noise induces QAM detection error which we note $\mathrm{P_e}$. The QAM detection error depends on the SNR_r level; a closed-form expression of $\mathrm{P_e}$ can be found in [21].

In the conventional approach for reference signal reconstruction, the noise-free signal is obtained by modulating the retrieved symbols $\hat{\mathbf{c}}$ as follows O'Hagan et al. [9,11,12,18–20]

$$\hat{\mathbf{s}} = \mathbf{F}^{-1}\mathbf{A}^T\hat{\mathbf{c}}_\mathbf{m}, \tag{23}$$

where $\hat{\mathbf{s}}$ is the reconstructed reference signal. Equivalently, we can write

$$\hat{\mathbf{s}} = \mathbf{p} + \hat{\mathbf{d}}, \tag{24}$$

where $\mathbf{p}$ is the pilot signal (perfectly reconstructed) and $\hat{\mathbf{d}}$ is the reconstructed data signal. The reconstructed reference signal, $\hat{\mathbf{s}}$, will replace the received reference signal for target detection.

3.3. Optimum reconstruction

In the conventional approach for reference signal reconstruction [9,11,18–20], the detected QAM symbols $\hat{\mathbf{c}}$ are employed to generate a noise-free reference signal. The reconstructed signal perfectly matches the transmitted signal for high SNR_r levels, i.e., negligible $\mathrm{P_e}$. For low SNR_r values, the QAM detection error is significant. Therefore, the reconstructed signal, based on the wrongly detected symbols, presents a mismatch with the transmitted signal. To deal with this issue, we propose to optimally filter the detected QAM symbols $\hat{\mathbf{c}}$ according to the SNR_r level. The optimum filter weights are calculated through the minimization of the mean square error (MSE) of the symbol estimation which we note J. For each symbol c, we have

$$J = \mathrm{E}\left[|h\hat{c} - c|^2\right], \tag{25}$$

where h is the filter weight, c is the exact symbol value, and $\hat{c}$ is the detected one. The optimum filter weight is calculated as follows Haykin [40]

$$h = \mathrm{E}\left[\hat{c}c^*\right]/\mathrm{E}\left[\hat{c}\hat{c}^*\right]. \tag{26}$$

The accuracy of the data symbol c_d detection depends on the SNR_r level as follows

$$\hat{c}_\mathrm{d} = c_\mathrm{d} \text{ with a probability of } (1 - \mathrm{P_e}). \tag{27}$$

In addition, for $\hat{c}_\mathrm{d} \neq c_\mathrm{d}$, we can write [12]

$$\mathrm{E}\left[\hat{c}_\mathrm{d}c_\mathrm{d}^*\right]_{\hat{c}_\mathrm{d}\neq c_\mathrm{d}} = 0, \tag{28}$$

it follows that

$$\mathrm{E}\left[\hat{c}_\mathrm{d} c_\mathrm{d}^*\right] = (1-\mathrm{P_e})\mathrm{E}\left[\hat{c}_\mathrm{d}\hat{c}_\mathrm{d}^*\right], \tag{29}$$

thus, the optimum filter weight for the detected QAM symbols is obtained as follows

$$h_\mathrm{d} = (1-\mathrm{P_e}). \tag{30}$$

Obviously, the pilot symbols (BPSK) do not require any filtering since they are fully known at the receiver. Therefore, the optimally filtered frequency-domain symbols are expressed as

$$\hat{\mathbf{c}}_\mathrm{opt} = \begin{pmatrix} (1-\mathrm{P_e})\hat{\mathbf{c}}_\mathrm{d} \\ \mathbf{c}_\mathrm{p} \end{pmatrix}. \tag{31}$$

Finally, the optimally reconstructed reference signal is obtained by

$$\hat{\mathbf{s}}_\mathrm{opt} = \mathbf{F}^{-1}\mathbf{A}^T\hat{\mathbf{c}}_\mathrm{opt}, \tag{32}$$

or equivalently,

$$\hat{\mathbf{s}}_\mathrm{opt} = \mathbf{p} + (1-\mathrm{P_e})\hat{\mathbf{d}}, \tag{33}$$

where $\mathrm{P_e}$ can be calculated employing the estimate of the reference signal signal-to-noise ratio $\hat{\mathrm{SNR}}_\mathrm{r}$ provided by (17).

4. Statistical analysis

In this section, we calculate closed-form expressions for the detection and the false-alarm probabilities relative to the considered system: a bistatic PCL radar based on DVB-T signals and with a reconstructed reference signal. To do so, we adopt the following generic model for the reconstructed reference signal

$$\hat{\mathbf{s}} = \mathbf{p} + a\hat{\mathbf{d}}, \tag{34}$$

where a is a positive real parameter, $\mathbf{p}$ is the pilot signal, and $\hat{\mathbf{d}}$ is the reconstructed data signal. Both $\mathbf{p}$ and $\hat{\mathbf{d}}$ are $(N\times 1)$ size arrays.

To calculate the detection and false-alarm probabilities, the detection statistic needs to be characterized. The detection test is executed as follows Liu et al. [16]

$$|\bar{T}|^2 \underset{\mathrm{H_0}}{\overset{\mathrm{H_1}}{\gtrless}} \lambda, \tag{35}$$

where $\bar{T}$ is the detection statistic and λ is the detection threshold.

Assuming that the detection test is performed at the target cell (τ, f_d). So, the reconstructed reference signal, $\hat{\mathbf{s}}$, is time-delayed by τ and frequency-shifted by f_d to be aligned with the target echo, we note the resulting signal as $\hat{\mathbf{s}}_\mathrm{t}$. The detection statistic is then given by

$$\bar{T} = \hat{\mathbf{s}}_\mathrm{t}^\dagger \mathbf{x}_\mathbf{s}, \tag{36}$$

where $\hat{\mathbf{s}}_\mathrm{t}$ is the reconstructed signal time-delayed and frequency-shifted, $\mathbf{x}_\mathbf{s}$ is the surveillance signal of length $N\times 1$. The detection statistic under the alternative hypothesis $(\mathrm{H_1})$ can be then expressed as

$$\bar{T} = (\mathbf{p}_\mathrm{t} + a\,\hat{\mathbf{d}}_\mathrm{t})^\dagger(\alpha(\mathbf{p}_\mathrm{t}+\mathbf{d}_\mathrm{t}) + \mathbf{w}), \tag{37}$$

it follows that

$$\bar{T} = \alpha(\mathbf{p}_\mathrm{t}^\dagger\mathbf{p}_\mathrm{t} + a\,\hat{\mathbf{d}}_\mathrm{t}^\dagger\mathbf{d}_\mathrm{t}) + \alpha(\mathbf{p}_\mathrm{t}^\dagger\mathbf{d}_\mathrm{t} + a\,\hat{\mathbf{d}}_\mathrm{t}^\dagger\mathbf{p}_\mathrm{t}) + (\mathbf{p}_\mathrm{t} + a\,\hat{\mathbf{d}}_\mathrm{t})^\dagger\mathbf{w}. \tag{38}$$

The statistic $\bar{T}$ is the sum of N i.i.d. samples, which allows to consider that $\bar{T}$ follows a Gaussian distribution with parameters (mean and variance) to be determined under both hypotheses $\mathrm{H_0}$ and $\mathrm{H_1}$. The mean value of the detection statistic is given by

$$\mathrm{E}\left[\bar{T}|\mathrm{H_1}\right] = \alpha(\mathbf{p}_\mathrm{t}^\dagger\mathbf{p}_\mathrm{t} + a\,\hat{\mathbf{d}}_\mathrm{t}^\dagger\mathbf{d}_\mathrm{t}), \tag{39}$$

this value is obtained considering that pilot signal and data signal are independent, which yields a null inter-correlation terms. We define the cross-covariance between the exact data signal and the reconstructed one as follows

$$\epsilon = \mathrm{E}\left[\hat{\mathbf{d}}_\mathrm{t}^\dagger\mathbf{d}_\mathrm{t}\right], \tag{40}$$

which can be expressed as

$$\epsilon = \mathrm{E}\left[\sum_{n=1}^{N}\hat{d}^*(n)d(n)\right], \tag{41}$$

where $d(n)$ and $\hat{d}(n)$ are the samples of the exact data signal and the reconstructed one, respectively. Since $\hat{d}(n)$ and $d(n)$ are both i.i.d., we can write

$$\epsilon = N\,\mathrm{E}\left[\hat{d}^*(n)d(n)\right], \tag{42}$$

employing the DVB-T signal model in Eq. (6), we can write

$$\epsilon = N\,\mathrm{E}\left[\sum_{k_1=1}^{K_\mathrm{d}}\sum_{k_2=1}^{K_\mathrm{d}} c_{k_1}\hat{c}_{k_2}^* e^{j2\pi f_{k_1} n} e^{-j2\pi f_{k_2} n}\right], \tag{43}$$

since the subcarriers are orthogonal, we can consider that

$$\mathrm{E}\left[c_{k_1}\hat{c}_{k_2}^* e^{j2\pi f_{k_1} n} e^{-j2\pi f_{k_2} n}\right]_{k_1\neq k_2} = 0, \tag{44}$$

it yields

$$\epsilon = N\,\mathrm{E}\left[\sum_{k=1}^{K_\mathrm{d}} c_k\hat{c}_k^*\right], \tag{45}$$

or simply

$$\epsilon = N\,K_\mathrm{d}\,\mathrm{E}\left[c_k\hat{c}_k^*\right], \tag{46}$$

if we use Eq. (29), we get

$$\epsilon = N\,K_\mathrm{d}(1-\mathrm{P_e})\mathrm{E}\left[\hat{c}_k\hat{c}_k^*\right], \tag{47}$$

knowing that the variance of the data signal is given by

$$\sigma_d^2 = K_\mathrm{d}\mathrm{E}\left[c_k c_k^*\right], \tag{48}$$

and

$$\mathrm{E}\left[c_k c_k^*\right] = \mathrm{E}\left[\hat{c}_k\hat{c}_k^*\right], \tag{49}$$

we can write

$$\epsilon = N(1-\mathrm{P_e})\sigma_d^2, \tag{50}$$

finally, the mean value of the detection statistic is expressed as

$$\mathrm{E}\left[\bar{T}|\mathrm{H_1}\right] = N\alpha\left(\sigma_p^2 + a(1-\mathrm{P_e})\sigma_d^2\right), \tag{51}$$

similarly, we can express the variance under the alternative hypothesis $(\mathrm{H_1})$ as

$$\begin{aligned}\mathrm{var}\left[\bar{T}|\mathrm{H_1}\right] = {} & N\left(|\alpha|^2\left(\sigma_p^4 + a^2(1-\mathrm{P_e})^2\sigma_d^4\right)\right. \\ & + |\alpha|^2\left(a^2 + 2a(1-\mathrm{P_e}) + 1\right)\sigma_d^2\sigma_p^2 \\ & \left. + \left(\sigma_p^2 + a^2\sigma_d^2\right)\sigma_w^2\right).\end{aligned} \tag{52}$$

Therefore, the mean and variance of the detection statistic $\bar{T}$ under the alternative hypothesis $(\mathrm{H_1})$ are given by

$$\mu_1 = \mathrm{E}\left[\bar{T}|\mathrm{H_1}\right], \tag{53}$$

$$\sigma_1^2 = \mathrm{var}\left[\bar{T}|\mathrm{H_1}\right]. \tag{54}$$

The parameters of $\bar{T}$ under the null hypothesis $(\mathrm{H_0})$ are obtained by setting $\alpha = 0$ in the expressions (51) and (52), which leads to

$$\mu_0 = 0, \tag{55}$$

$$\sigma_0^2 = N\left(\left(\sigma_p^2 + a^2\sigma_d^2\right)\sigma_w^2\right). \tag{56}$$

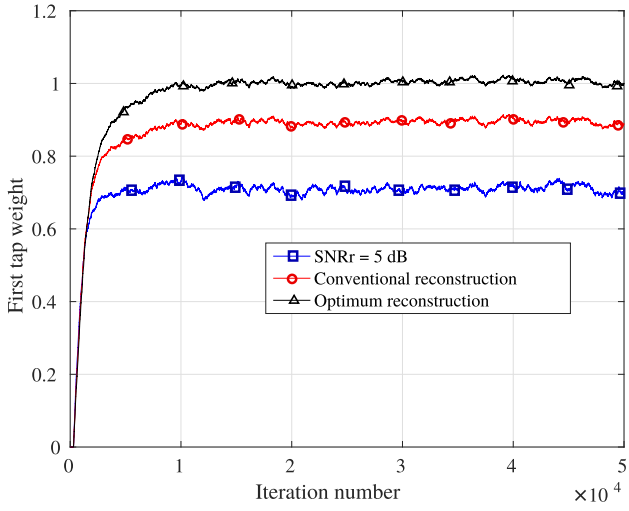

(a) $SNR_r = 5$ dB.

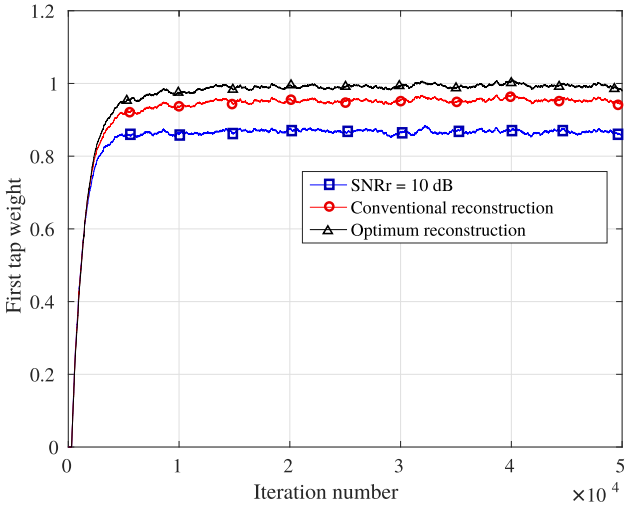

(b) $SNR_r = 10$ dB.

Fig. 4. Impact of the reference signal quality on the LMS convergence.

Knowing the parameters of $\bar{T}$ under both hypotheses, we can calculate the false-alarm probability P_{FA} and the detection probability P_D as follows Liu et al. [16]

$$P_{FA} = \exp(-\lambda/\sigma_0^2), \tag{57}$$

and

$$P_D = Q_1\left(\sqrt{\frac{2|\mu_1|^2}{\sigma_1^2}}, \sqrt{\frac{2\sigma_0^2 \log(P_{FA}^{-1})}{\sigma_1^2}}\right). \tag{58}$$

To obtain the detection probability for the conventional reconstruction, we set $a = 1$. For the optimum reconstruction we set $a = 1 - P_e$. When employing a pilot signal for detection, the detection probability is calculated by considering $a = 0$ [41].

5. Results and discussion

In this section, we present simulation and real-data results to validate the proposed methods and to evaluate their performances.

5.1. Simulation results: static-clutter suppression efficiency

In this section, we evaluate the quality of the reconstructed signal by measuring the static-clutter suppression (SCS) efficiency. In order to do so, we consider the adaptive least mean squares (LMS) as a SCS approach and we investigate the estimation convergence of the direct-path signal weight which we set as $h_0 = 1$ (3). Fig. 4 presents the results for two SNR_r values where three variants of the reference signal are considered: noisy, conventionally reconstructed, and optimally reconstructed.

Firstly, we notice that reference signal noise induces an estimation error of the filter weights, which will result in a residual static-clutter contribution in the filtered surveillance signal. Secondly, we remark that both signal reconstruction methods reduce the estimation error, which improves the SCS performance. However, the optimum reconstruction outperforms the conventional approach for the reduction of the estimation error. Thus, the proposed method for reference signal reconstruction can improve the PCL radar performances by allowing an efficient SCS (in addition to the detection probability enhancement).

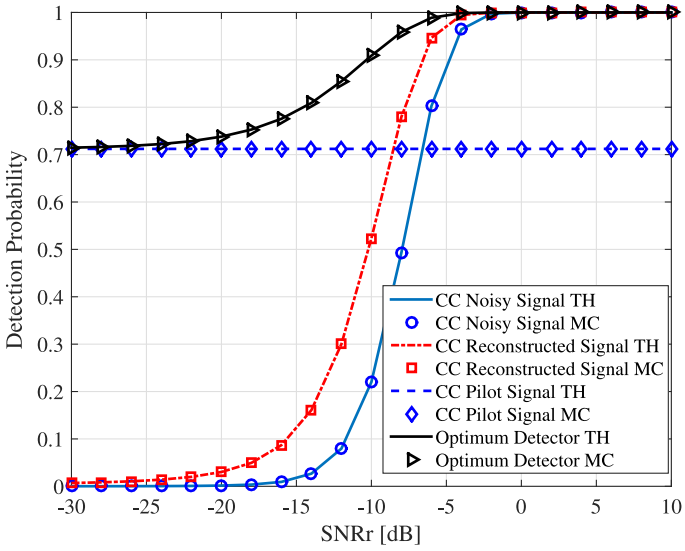

Fig. 5. Monte-Carlo and theoretical results for the detection probability as a function of SNR_r for $SNR_s = -32$ dB, $N = 10^5$, and $P_{FA} = 10^{-4}$.

5.2. Simulation results: detection probability

5.2.1. Results for one SNR_s value

We start with the validation of the retrieved expressions for detection and false-alarm probabilities. In order to do so, we performed Monte-Carlo (MC) simulations with the following parameters: number of trials $N_{trials} = 10^6$, false-alarm probability $P_{FA} = 10^{-4}$, coherent processing interval length $N = 10^5$, and a signal-to-noise ratio in the surveillance signal $SNR_s = -32$ dB. Fig. 5 presents both MC and theoretical results for the detection probability. Four detection strategies are examined; each strategy is characterized by the reference signal model employed for the detection. The four reference signal variants are: a noisy signal, a conventionally reconstructed signal ($a = 1$), a pilot signal ($a = 0$), and an optimally reconstructed signal ($a = 1 - P_e$). A perfect match can be noticed between Monte-Carlo results and the theoretical ones, which validates the retrieved expressions for detection and false-alarm probabilities.

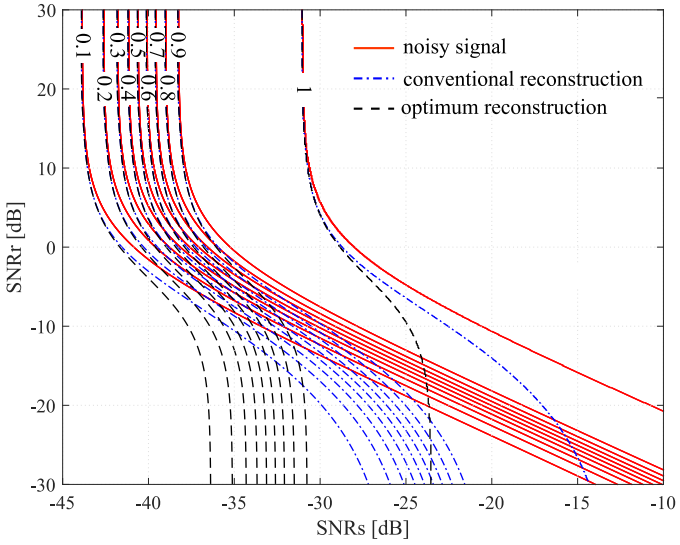

Fig. 6. Detection probability as a function of SNR_r and SNR_s for $N = 10^5$, and $P_{FA} = 10^{-4}$.

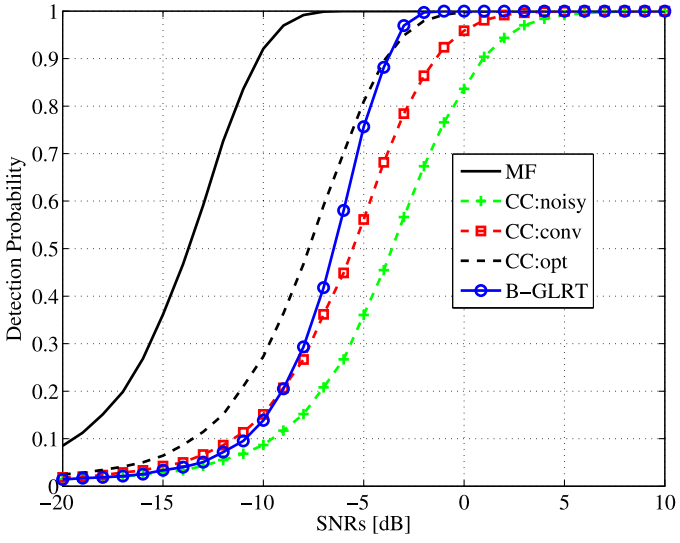

Fig. 7. Detection probability as a function of SNR_s for $SNR_r = -10$ dB, $N = 100$, and $P_{FA} = 10^{-2}$.

As can be seen, the reference signal noise degrades the detection probability. Also, we notice that the conventional reconstruction of the reference signal improves the detection probability. However, for low SNR_r values, the conventional reconstruction loses its capabilities due to the significant QAM detection error. It falls behind the detection method that employs pilot signal for $SNR_r < -10$ dB.

The pilot signal is generated at the receiver, which leads to an independent behavior of the detector employing a pilot signal towards SNR_r values. This detection strategy can replace the conventional reconstruction method for $SNR_r < -10$ dB since the reconstruction noise caused by QAM detection error is larger than the loss of the coherent processing gain related to the use of one component of the signal.

The detection strategy which employs an optimally reconstructed reference signal offers the best results in terms of detection probability. Filtering the detected QAM symbols permits an optimum control of the contribution of the data signal, which reduces the mismatch between the reconstructed signal and the exact one. For low SNR_r values, the optimum detector behavior tends

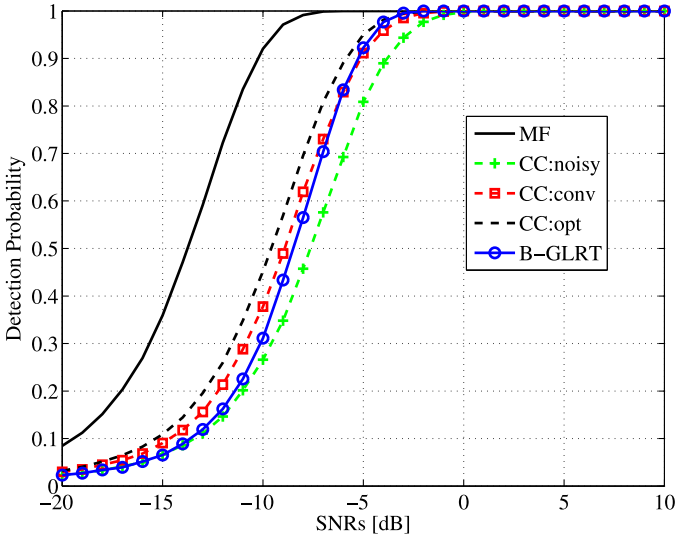

Fig. 8. Detection probability as a function of SNR_s for $SNR_r = -5$ dB, $N = 100$, and $P_{FA} = 10^{-2}$.

to the one of the method using a pilot signal since $P_e \approx 1$ which causes a full suppression of the data signal from the reconstructed signal. For high SNR_r values, the QAM detection error is negligible, thus, the optimum detector results fit with the ones of the conventional reconstruction strategy ($P_e \approx 0$).

5.2.2. Results for many SNR_s values

Considering a unique value of SNR_s for comparing the detection probability in the conventional and optimum reconstruction schemes provides a limited vision about the detection performances. To obtain a larger insight, we calculate the detection probability for different pairs of SNR_s and SNR_r values with a false-alarm probability of $P_{FA} = 10^{-4}$. Fig. 6 presents the detection probability contours for three detection strategies: a noisy reference signal, a conventionally reconstructed signal, and an optimally reconstructed signal.

Firstly, we notice that the three methods provide the same detection probability value (for a given SNR_s value) for $SNR_r > 10$ dB, which means that the impact of the reference signal noise is insignificant. In addition, the detection probability seems to be independent of the SNR_r value, which is similar to the matched filter detector behavior. This can be argued by the large coherent processing interval employed which reduces the noise-floor level.

Secondly, we remark that for $0\,\text{dB} < SNR_r < 10\,\text{dB}$, the conventional and the optimum reconstruction methods provide the same performance which is higher than the noisy reference signal case. In this case, the QAM detection error does not significantly affect the detection probability, consequently, the designed filter impact is negligible. Thus, the filtered signal behaves like the conventionally reconstructed one.

Thirdly, for $SNR_r < 0$ dB, the optimum reconstruction method significantly outperforms the conventional reconstruction method for all SNR_s values, which is the result of the optimum filtering of the detected QAM symbols. The QAM symbol filtering reduces the mismatch between the reconstructed signal and the exact one, and thus maximizes the coherent processing gain.

Finally, we note that for $SNR_r < -20$ dB, the behavior of the optimum reconstruction depends only on the SNR_s value, which is similar to the behavior of the detector employing pilot signal. For these SNR_r values, the QAM detection error approaches the value 1, which forces the filter to exclude the data symbols from the reconstructed signal.

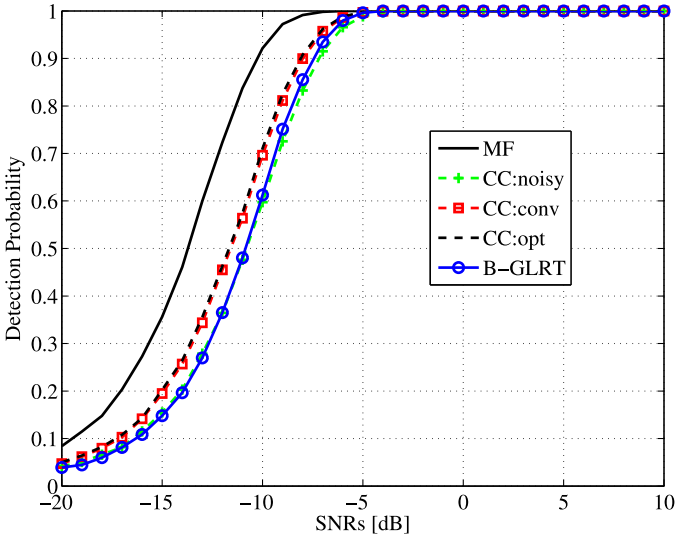

Fig. 9. Detection probability as a function of SNR_s for $SNR_r = 0$ dB, $N = 100$, and $P_{FA} = 10^{-2}$.

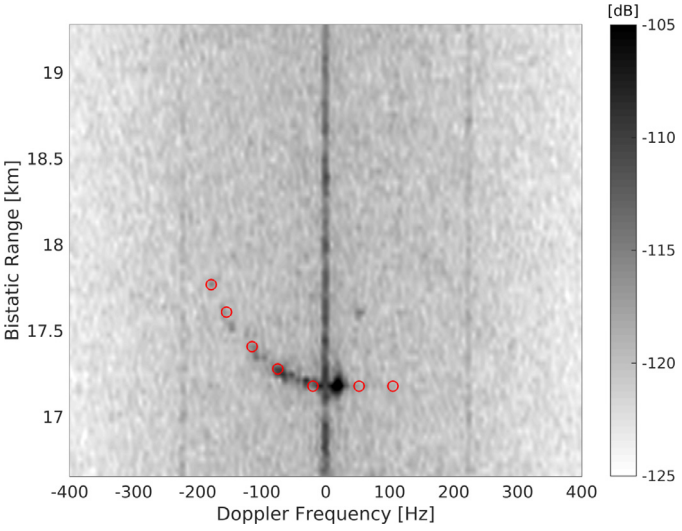

Fig. 11. Real-data results of summed RDDs for a conventionally reconstructed reference signal with an initial $SNR_{r=3.8\ dB}$ and a coherent integration interval of duration $T = 0.1$ s.

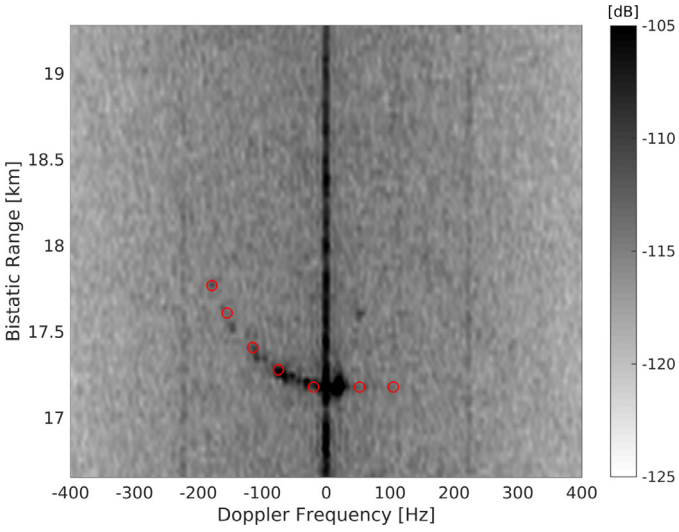

Fig. 10. Real-data results of summed RDDs for a noisy reference signal with $SNR_{r=3.8\ dB}$ and a coherent integration interval of duration $T = 0.1$ s. (For interpretation of the references to color in this figure, the reader is referred to the web version of this article.)

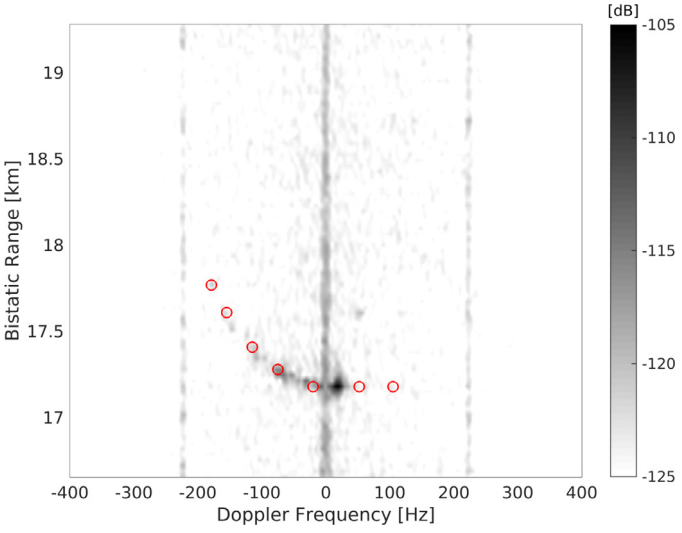

Fig. 12. Real-data results of summed RDDs for an optimally reconstructed reference signal with an initial $SNR_{r=3.8\ dB}$ and a coherent integration interval of duration $T = 0.1$ s.

5.2.3. Comparison with the GLRT detector

The previous detection probability results have shown the efficiency of the optimum signal reconstruction in dealing with noisy reference signal scenarios. In [14], a set of four detection algorithms have been proposed for the detection with a noisy reference signal scenario. These algorithms are based on the generalized likelihood ratio test (GLRT) principle. They are derived following the four combinations of: known/unknown noise power and deterministic/stochastic signal. The algorithm that corresponds to our case in noted as B-GLRT, where the noise power is known and the signal is stochastic; since the DVB-T signal can be modeled as a complex Gaussian and the noise power can be estimated as presented in Section 2. To compare the performances of the signal reconstruction to the B-GLRT algorithm, we considered the simulation parameters employed in [14] with $N = 100$, $P_{FA} = 10^{-2}$ and three values of SNR_r: $\{-10\ dB, -5\ dB, 0\ dB\}$. The results of the detection probability as a function of SNR_s are presented in Figs. 7, 8 and 9, respectively.

Fig. 7 presents the detection probability results for $SNR_r = -10$ dB. In this scenario, the B-GLRT algorithm outperforms the conventional reconstruction. However, the optimum reconstruction achieves better performances than the B-GLRT for $SNR_s < -4$ dB. For $SNR_r = -5$ dB and $SNR_r = 0$ dB (Figs. 8 and 9), both signal reconstruction methods outperform the B-GLRT algorithms by achieving larger detection probability results. Again, we validate the efficiency of the optimum DVB-T signal reconstruction for the enhancement of the detection probability.

5.3. Real-data results

5.3.1. Comparison of the signal reconstruction methods

To validate the theoretical and simulation results, we apply the reconstruction methods on real-data sets. The measurement campaign was performed in Brussels at the Royal Military Academy (RMA). We considered the DVB-T transmitter located at Veltem with a distance of 16 km from the receiver site and with a reference signal of $SNR_{r=3.8\ dB}$. The proximate Zaventem airport (BRU),

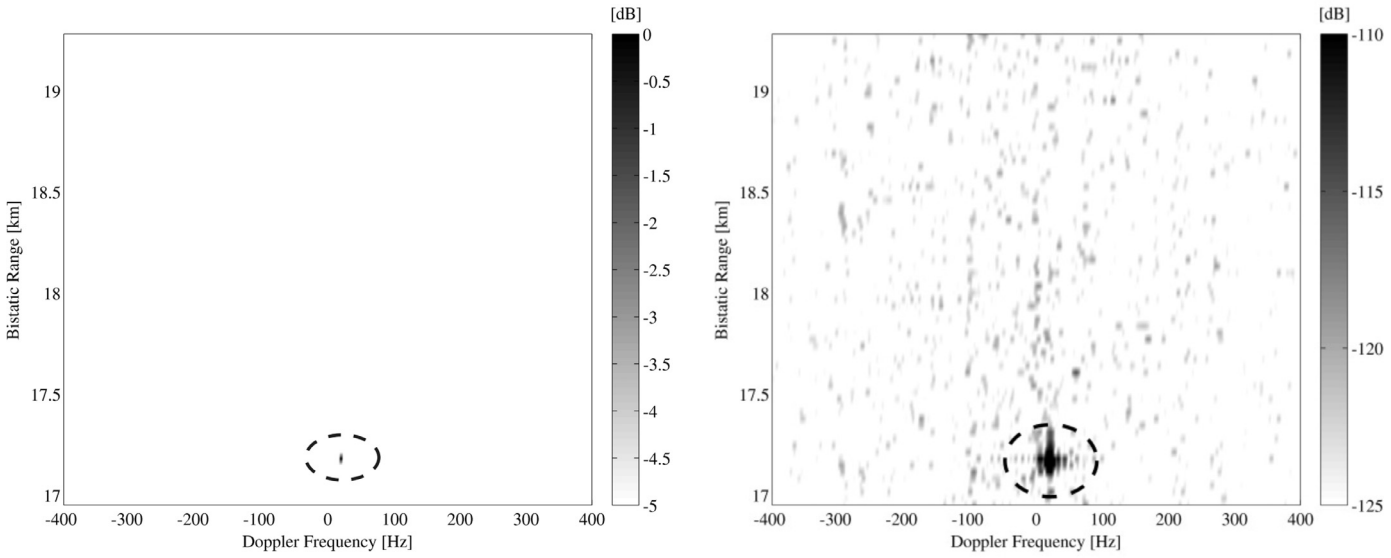

(a) B-GLRT algorithm with noisy reference signal. (b) Optimally reconstructed reference signal.

Fig. 13. Range-Doppler diagrams for a real data-set with a target echo located at (17.18 km, 20 Hz) and a coherent integration interval of duration $T = 0.1$ s.

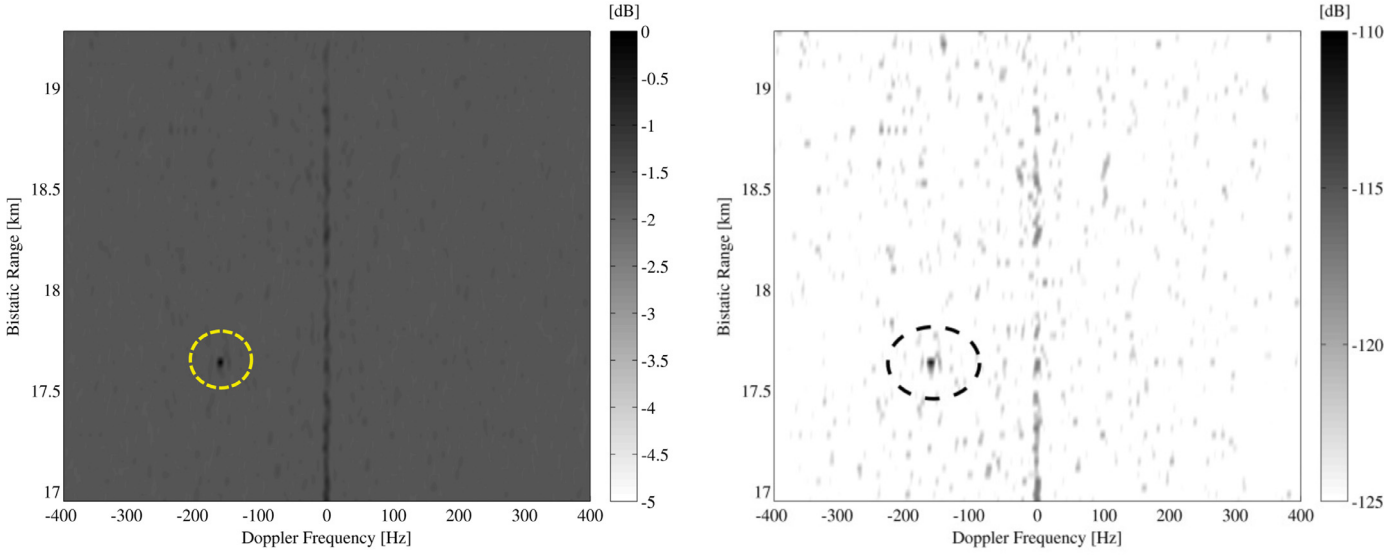

(a) B-GLRT algorithm with noisy reference signal. (b) Optimally reconstructed reference signal.

Fig. 14. Range-Doppler diagrams for a real data-set with a target echo located at (17.65 km, −160 Hz) and a coherent integration interval of duration $T = 0.1$ s.

10 km from the receiver, offers the possibility of having low-altitude targets during landing and taking off maneuvers. The reception channel includes a Yagi antenna (MXR0012), a USRP B100 device, and a computer running GNU radio software. To obtain a ground-truth information about the exact location of the targets, we simultaneously recorded ADS-B signals which corresponds to the airplanes overflying the surveillance area.

Fig. 10 presents the sum of consecutive range-Doppler diagrams which shows the airplane path; the received reference signal is employed in this case. ADS-B results are shown also in the figure to indicate the exact positions of the airplane (red circles). We notice that the airplane track is barely distinguishable due to the masking effect of the noise-floor induced by the reference signal noise.

To reduce the impact of the reference signal, we conventionally reconstruct the received signal; the result is presented in Figs. 11. We remark that the conventional reconstruction has reduced the noise-floor level by about 5 dB, which improves the range-Doppler diagram quality and thus the target detectability.

Fig. 12 presents the results for an optimally reconstructed reference signal. We notice that this approach enabled a noise-floor reduction of more than 10 dB, which proves the advantage of the proposed method over the conventional reconstruction approach.

5.3.2. Comparison with the B-GLRT detector

Since the estimated value of $\mathrm{SNR_r}$ is 3.8 dB, the difference between the optimum signal reconstruction and the B-GLRT algorithm may not be significant. We propose to investigate the performance of B-GLRT for a noisy reference signal using real data-sets. In order to so, we consider two data-sets for different $\mathrm{SNR_s}$ values (two values of the bistatic range). The detection results are presented in Figs. 13 and 14.

Fig. 13 presents the corresponding results to the case where the target is located at (17.18 km, 20 Hz). In this case, both methods provide acceptable results, where the target is distinguishable from the noise-floor level. We note that for the GLRT results, we show the RDD normalized to its maximum value. In Fig. 14, we show the RDD results for a target with a relatively low SNR_s compared to the first case. For both methods, the target is distinguishable, however, the B-GLRT results are characterized by a considerable noise-floor level. This emphasizes the limitation of the B-GLRT algorithm due to the lower dynamic range of the detector output compared to the CC detector.

6. Conclusion

In this paper, we provided an analytic assessment of the reference signal reconstruction approach for DVB-T based PCL radars. Two methods were studied: the conventional and the proposed optimum methods. Analytic expressions for the detection and false-alarm probabilities were derived and validated through Monte-Carlo simulations. In addition, real-data sets were employed to evaluate the impact of both methods on the detection performances. The conventional method is limited for low SNR values since it includes a mismatch aspect in the reconstructed signal due to the QAM symbol detection error. The proposed method filters the detected QAM symbols to reduce the reconstruction mismatch. For both simulation and real-data results the proposed method outperforms the conventional one. Thus, the proposed method can extend the feasibility of the reference signal reconstruction approach for low SNR values, which enables the use of distant DVB-T transmitters as illuminators of opportunity.

References

[1] N.J. Willis, Bistatic Radar, SciTech Pub, 2005.
[2] H.D. Griffiths, C.J. Baker, Measurement and Analysis of Ambiguity Functions of passive Radar Transmissions, Institute of Electrical and Electronics Engineers Inc, 2005, pp. 321–325.
[3] C.J. Baker, H.D. Griffiths, I. Papoutsis, Passive coherent location radar systems. part 2: waveform properties, IEE Proc. Radar Sonar Navig. 152 (3) (2005) 160.
[4] P. Howland, D. Maksimiuk, G. Reitsma, FM Radio based bistatic radar, IEE Proc. Radar Sonar Navig. 152 (3) (2005) 107.
[5] C. Bongioanni, F. Colone, P. Lombardo, Performance analysis of a multi-frequency FM based passive bistatic radar, in: Proceedings of the IEEE Radar Conference, IEEE, 2008, pp. 1–6.
[6] M. Malanowski, K. Kulpa, J. Kulpa, P. Samczynski, J. Misiurewicz, Analysis of detection range of FM-based passive radar, IET Radar Sonar Navig. 8 (2) (2014) 153–159.
[7] M. Kubica, V. Kubica, X. Neyt, J. Raout, S. Roques, M. Acheroy, Optimum target detection using illuminators of opportunity, in: Proceedings of the IEEE Conference on Radar, 2006, p. 8 pp..
[8] X. Neyt, J. Raout, M. Kubica, V. Kubica, S. Roques, M. Acheroy, J.G. Verly, Feasibility of STAP for passive GSM-based radar, in: Proceedings of the IEEE Conference on Radar, 2006, p. 6pp..
[9] D.W. O'Hagan, H. Kuschel, J. Heckenbach, M. Ummenhofer, J. Schell, Signal reconstruction as an effective means of detecting targets in a DAB-based PBR, in: Proceedings of the Eleventh International Radar Symposium, 2010, pp. 1–4.
[10] M. Daun, U. Nickel, W. Koch, Tracking in multistatic passive radar systems using DAB/DVB-T illumination, Signal Process. 92 (6) (2012) 1365–1386.
[11] C.R. Berger, B. Demissie, J. Heckenbach, P. Willett, S. Zhou, Signal processing for passive radar using OFDM waveforms, IEEE J. Sel. Top. Signal Process. 4 (1) (2010) 226–238.
[12] J.E. Palmer, H.A. Harms, S.J. Searle, L.M. Davis, DVB-T passive radar signal processing, IEEE Trans. Signal Process. 61 (2013) 2116–2126.
[13] G. Cui, J. Liu, H. Li, B. Himed, Target detection for passive radar with noisy reference channel, in: Proceedings of the IEEE Radar Conference, 2014, pp. 144–148.
[14] G. Cui, J. Liu, H. Li, B. Himed, Signal detection with noisy reference for passive sensing, Signal Process. 108 (2015).
[15] M.K. Bączyk, K. Kulpa, P. Samczyński, M. Malanowski, The impact of reference channel SNR on targets detection by passive radars using DVB-T signals, in: Proceedings of the IEEE Radar Conference (RadarCon), 2015, pp. 708–712.
[16] J. Liu, H. Li, B. Himed, On the performance of the cross-correlation detector for passive radar applications, Signal Process. 113 (2015).
[17] X. Zhang, H. Li, B. Himed, Multistatic passive detection with parametric modeling of the IO waveform, Signal Process. 141 (2017) 187–198.
[18] M.K. Baczyk, M. Malanowski, Decoding and reconstruction of reference DVB-T signal in passive radar systems, in: Proceedings of the Eleventh International Radar Symposium (IRS), 2010, pp. 1–4.
[19] S. Searle, S. Howard, J. Palmer, Remodulation of DVB-T signals for use in passive bistatic radar, in: Proceedings of the Conference Record of the Forty Fourth Asilomar Conference on Signals, Systems and Computers (ASILOMAR), 2010, pp. 1112–1116.
[20] M. Baczyk, M. Malanowski, Reconstruction of the reference signal in DVB-T-based passive radar, Int. J. Electron. Telecommun. 57 (1) (2011) 43–48.
[21] J.R. Barry, E.A. Lee, D.G. Messerschmitt, E.A. Lee, Digital Communication, Springer, 2004.
[22] O. Mahfoudia, F. Horlin, X. Neyt, Optimum reference signal reconstruction for DVB-T based passive radars, in: Proceedings of the IEEE Radar Conference (RadarConf), 2017.
[23] F. Wang, H. Li, X. Zhang, B. Himed, Signal parameter estimation for passive bistatic radar with waveform correlation exploitation, IEEE Trans. Aerosp. Electron. Syst. 54 (2018) 1135–1150.
[24] F. Colone, D.W. O'Hagan, P. Lombardo, C.J. Baker, A multistage processing algorithm for disturbance removal and target detection in passive bistatic radar, IEEE Trans. Aerosp. Electron. Syst. 45 (2009) 698–722.
[25] C. Schwark, D. Cristallini, Advanced multipath clutter cancellation in OFDM-based passive radar systems, in: Proceedings of the IEEE Radar Conference (RadarConf), IEEE, 2016, pp. 1–4.
[26] O. Mahfoudia, F. Horlin, X. Neyt, On the static clutter suppression for DVB-T based passive radars, in: Proceedings of the Thirty-Second URSI General Assembly and Scientific Symposium, Montreal, Canada, 2017.
[27] E. JTC, Digital video broadcasting (DVB);framing structure, channel coding and modulation for digital terrestrial television, Technical Report, Stadard, 2004.
[28] H. Ochiai, H. Imai, On the distribution of the peak-to-average power ratio in OFDM signals, IEEE Trans. Commun. 49 (2) (2001) 282–289.
[29] S. Shepherd, J. Orriss, S. Barton, Asymptotic limits in peak envelope power reduction by redundant coding in orthogonal frequency-division multiplex modulation, IEEE Trans. Commun. 46 (1) (1998) 5–10.
[30] R. Saini, M. Cherniakov, DTV Signal ambiguity function analysis for radar application, IEE Proc. Radar Sonar Navig. 152 (3) (2005) 133.
[31] I. Kotzer, S. Har-Nevo, S. Sodin, S. Litsyn, A Model for OFDM signals with applications, in: Proceedings of the European Wireless 2012; Eighteenth European Wireless Conference, 2012, pp. 1–7.
[32] A. Rudzinski, Normalized gaussian approach to statistical modeling of OFDM signals, J. Telecommun. Inform. Technol. nr 1 (2014) 54–61.
[33] A.Y. Gafer, S. Elsadig, J. Varun, Front-end signal to noise ratio estimation for DVBT fixed reception in flat-fading channel, in: Proceedings of the Fourth International Conference on Intelligent and Advanced Systems (ICIAS), 1, 2012, pp. 296–300.
[34] J. van de Beek, M. Sandell, P. Borjesson, ML Estimation of time and frequency offset in OFDM systems, IEEE Trans. Signal Process. 45 (1997) 1800–1805.
[35] D.-K. Kim, S.-H. Do, H.-K. Lee, H.-J. Choi, Performance evaluation of the frequency detectors for orthogonal frequency division multiplexing, IEEE Trans. Consum. Electron. 43 (3) (1997) 776–783.
[36] S. Fechtel, OFDM Carrier and sampling frequency synchronization and its performance on stationary and mobile channels, IEEE Trans. Consum. Electron. 46 (3) (2000) 438–441.
[37] S.-H. Chen, W.-H. He, H.-S. Chen, Y. Lee, Mode detection, synchronization, and channel estimation for DVB-T OFDM receiver, in: Proceedings of the IEEE Global Telecommunications Conference (IEEE Cat. No.03CH37489), 5, IEEE, 2003, pp. 2416–2420.
[38] M. Rotoloni, S. Tomasin, L. Vangelista, Maximum likelihood estimation of time and carrier frequency offset for DVB-T2, IEEE Trans. Broadcast. 58 (2012) 77–86.
[39] X. Zhang, J. Liu, H. Li, B. Himed, Maximum likelihood synchronization for DVB-T2 in unknown fading channels, IEEE Trans. Broadcast. 61 (2015) 615–624.
[40] S. Haykin, Adaptive Filter Theory (3rd Ed.), Upper Saddle River, NJ, USA: Prentice-Hall, Inc., 1996.
[41] O. Mahfoudia, F. Horlin, X. Neyt, Target detection for DVB-T based passive radars using pilot subcarrier signal, in: Proceedings of the Thirty-Seventh WIC Symposium on Information Theory in the Benelux, 2016.